Surface failure mode evaluation of pure AlN and AlN with Al_2O_3(0.1 μm) oxide layer by microscratch testing

LOTFI CHOUANINE*, MASAYUKI TAKANO, FUMIO ASHIHARA, OSAMU KAMIYA
Department of Mechanical Engineering,Faculty of Engineering & Resource Science, Akita University, 010-8502 Akita, Japan
E-mail: tulotfi@ipc.akita-u.ac.jp

Published online: 25 August 2005

The surface scratch resistance, damage evolution and damage detection during microscratching of pure AlN and AlN with an Al_2O_3 oxide layer ($\sim$0.1 μm) were investigated. The microscratch experiments were performed in a progressive load-ramped mode where the load was linearly increased from 0 to 3 N as the scratch progressed with a loading rate of 0.2 N/min. The experiments resulted to two different failure mechanisms; Ductile scratching and fracture dominated scratching. In the case of pure AlN, inconsistent different kinds of damages were found to initiate at low critical load measured as 0.30 N. This critical load was also found to decrease with increasing the surface roughness, material density and grain size of AlN. In the case of pure AlN with an Al_2O_3 oxide layer, the critical load for crack initiation was measured as 0.45 N, higher than pure AlN. This critical load was found to generate uniform discontinuous chipping. The distance between these defects decreased and the failure mode gradually transformed to continuous chipping as the scratch progressed. The surface modification of AlN with the use of an Al_2O_3 oxide layer was found to improve the tribological properties of AlN.
© *2005 Springer Science + Business Media, Inc.*

1. Introduction

Increasingly, high performance ceramics are finding wide range of applications such as in semiconductor processing components, which provide fixtures of silicon wafers in vacuum environments without the use of mechanical clamps. Besides widely known sapphire, AlN-based electrostatic chuck (EC) device, which holds and often heats the silicon wafer during plasma chemical vapor deposition [1, 2], possess many attractive characteristics, e.g., good dielectric strength (20 kV/mm), low thermal expansion coefficient close to that of silicon (2.5×10^{-6} K^{-1}), high thermal conductivity (320 W/m·K), high melting point ($\sim$2700 K), non-reactive with normal semiconductor process chemicals and gases [3, 4].

However, residual stress/strain and defect density control during processing and polishing of AlN [5] is a major problem to be solved. The excellently balanced features of AlN for semiconductors equipment applications are directly affected by the surface defects of the material. In harsh high temperature vacuum environment, the chucking force on the 340 mm diameter AlN-based EC produces a stress of 15 kPa if the surface of the device is smoothly polished and $\sim$5 kPa if the surface of the device is roughly polished. The problem of surface defects on AlN which cause degradation of the chucking force and de-chucking time of AlN based EC in harsh vacuum environment can be solved by the reconsideration of the material fabrication process and the development of advanced adequate and robust ultra-precision finishing technology capable of removing the surface of AlN without inducing defects. However, this is time consuming and costly process.

It was decided in this work to oxide the AlN samples with a homogeneous Al_2O_3 oxide layer of $\sim$0.1 μm in thickness, so that to cover the surface damages as well as the sub-surface damages [5] in the material and therefore to insure uniform area of the AlN-based EC in contact with the silicon wafer backside during plasma etching process and to avoid the degradation of the temperature uniformity [6–8]. Accordingly, it was necessary to use tribological testing techniques [9–20] such as microscratch testing to assess the changes in the surface properties between AlN and AlN with an Al_2O_3 oxide layer. Microscratch testing is a comprehensive method of quantifying

*Author to whom all correspondence should be addressed.

0022-2461 © *2005 Springer Science + Business Media, Inc.*
DOI: 10.1007/s10853-005-0946-7

TABLE I Properties of AlN

Features		Pure AlN (Sintering aidless)	AlN (Y_2O_3-doped)	High pure AlN (Sintering aidless)
Purity	%	99.5	–	>99.9
Density	g/cm^3	3.26	3.27	3.33
Grain size	μm	3.0	5.9	9.8
Y	%	0.0	3.3	0.0
O	%	0.58	1.2	0.66
Total metal impurities	ppm	<500	<500	<200
Flextural strength	MPa	360	372	280
Vickers hardness	GPa	11.58	10.4	9.43
Young modulus	GPa	310	320	321
Fracture toughness	MPa.m$^{1/2}$	2.2	2.8	3.8
Thermal conductivity	W/m·K	90	200	80

*The material properties are from Ostech [21]

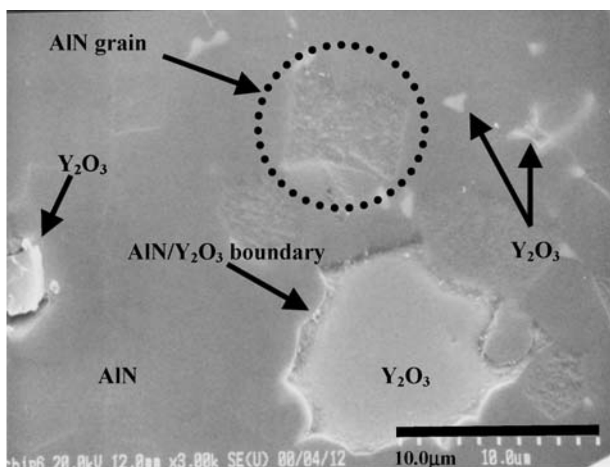

Figure 1 SEM image showing the surface topography of Y_2O_3 (Yttria)-doped AlN sample as received.

the scratch resistance, cohesion (mechanical durability) and adhesion (delamination) of a wide range of ceramic substrates and substrate/film systems [9–11]. The technique involves generating a controlled scratch with a diamond stylus on the AlN sample under test. This is achieved by pressing a diamond stylus on the sample surface with a progressive normal load (F_N) at the same time with displacing the AlN sample at a constant speed. At a given load, the AlN deformation generates stresses resulting to permanent cohesive damages such as chipping and cracking. The smallest load at which a specific failure event was recorded is called the critical load (F_C).

In this paper, details of microscratch experiments aimed at identifying the cohesion failure mode of different types of AlN and AlN with an Al_2O_3 oxide layer are discussed.

2. Experimental details

2.1. Samples

The AlN samples we used in the current work are processed using sintering additives and hot isostatic press technology and designed for semiconductors equipment applications. The general properties of these AlN samples shown in Table I are from Ostech electronic materials catalog [21]. The surface roughness of the substrates as received was measured by a white-light interferometer (NewView5000, 0.25 × .025 mm^2, 100 × objective, 0.1 nm vertical resolution, 10 measurements per surface) and was evaluated to be ∼0.25 μm (Ra).

In the first series of the microscratch experiments, three different AlN substrates were tested; Pure AlN, high pure AlN, and a Y_2O_3 (Yttria)-doped AlN consisting of 3.3% Yttrium, 1.2% oxygen and total metal impurities less than 500 ppm. Fig. 1 shows the SEM micrograph using backscattered electrons of the surface topography of the Y_2O_3-doped AlN as received. The elemental composition of the sample was performed using energy dispersive X-ray analysis.

In the second series of the microscratch experiments, three more separate AlN samples with homogeneous Al_2O_3 oxide layers (∼0.1 μm in thickness) were tested; AlN(Pure)/Al_2O_3, AlN(High pure)/Al_2O_3, and a AlN(Y_2O_3-doped)/Al_2O_3. These samples were first ultrasonically cleaned in acetone and ethyl alcohol then they were oxidized through a heat treated in a

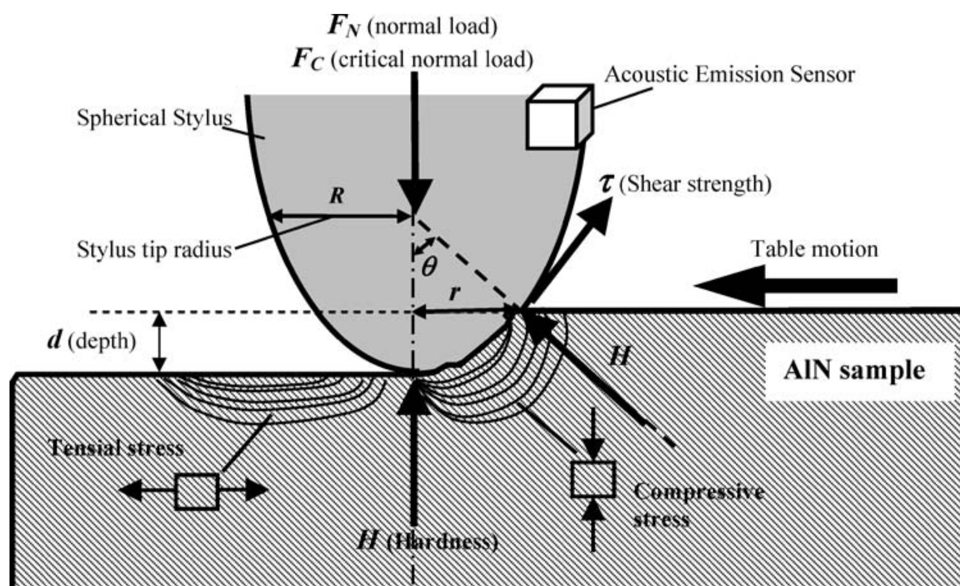

Figure 2 Geometry of the microscratch test showing the forces acting on tip of the diamond stylus.

tube furnace (heating rate 5°C/min.) for 6 min in flowing O_2 (Matheson, UHP) at 1250°C. The oxidation process was followed by an annealing procedure in direct cooling to room temperature under flowing Ar. The thickness of the Al_2O_3 oxide layers were measured by the spherical abrasion test method (Calowear, CSM, 2 measurements per sample) [22] and was found to be equal to ~0.1 μm.

2.2. Microscratch experimental conditions

The microscratch experiments were performed on AlN and AlN/Al_2O_3 samples using a micro scratch tester (CSM, Switzerland) equipped with an acoustic emission sensor and operated in the progressive normal load mode. The testing method, which is schematically shown in Fig. 2, consisted of pressing a Rockwell spherical type diamond stylus of tip radius (R) equal to ~10 μm with a normal load F_N in the range from 0 to 3 N (For clarification, the iso-stress contours around the diamond stylus shown in Fig. 2 are only the author's conception of the scratch mechanism). While a load was applied, the sample was moved at a constant speed of 0.401 mm/min and a loading rate of 0.2 N/min. The total length of the scratch was equal to 6 mm. These microscratch experimental conditions were kept unchanged during testing all samples. Three microscratch measurements per sample were performed and statistical methods were used to de-convolute the results.

Cross-referenced data on the smallest load at which a specific failure event was recorded, i.e., the critical load for fracture initiation and propagation F_C, were evaluated within a statistical deviation of ±0.01 N by simultaneously recording three different effects; Tangential force variations, acoustic emission (AE) fluctuations, and microscopic deformations. At a critical load F_C, the surface deformations of the AlN sample generated stresses which resulted to permanent cohesive damages such as chipping and cracking. For the scratch geometry shown in Fig. 2, the surface hardness (H) and shear strength (τ) of AlN are given by [9]

$$H = \frac{F_C}{\pi \cdot r^2}, \quad \tau = H \tan\theta = \frac{F_C}{\pi \cdot r^2}\left[\frac{r}{(R^2 - r^2)^{\frac{1}{2}}}\right] \tag{1}$$

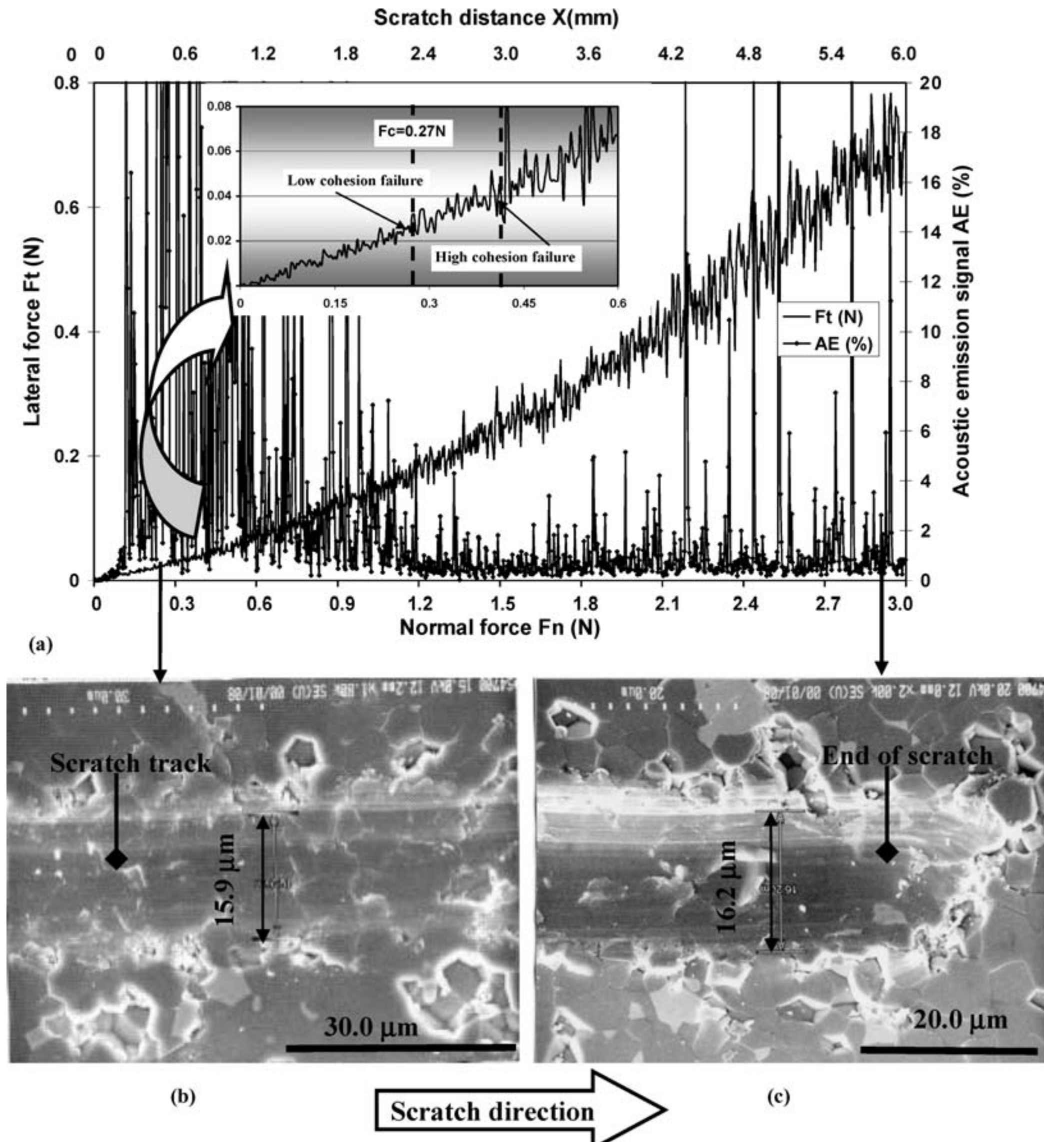

Figure 3 Results of microscratch test on Y_2O_3-doped AlN sample. (a) Lateral force (F_T) and acoustic emission signal intensity versus normal load (F_N) curves. (b) and (c) SEM images of the scratch tracks corresponding to critical load $F_C = 0.27$ N and maximum normal load $F_N = 3$ N, respectively.

TABLE II Average measured critical load F_C (±0.01 N) and shear strength τ for cohesive failure of AlN and AlN with Al_2O_3 oxide layer (three tests per sample)

	Surface condition		Microscratch results			
Type of AlN substrate	Roughness Ra (μm)	Oxidation Al_2O_3 (μm)	Critical load F_C (±0.01N)	Contact radius r (μm)	Shear strength τ (MPa)	Fracture failure mode
AlN	∼0.25	–	0.30	6.00	1989	Inconsistent cracks
(Pure)	∼0.05	–	0.35	5.97	2321	Inter-granular lateral cracks
	∼0.25	∼0.1	0.45	4.55	3536	Uniform chipping
AlN	∼0.25	–	0.27	7.95	1790	Inconsistent cracks
(Y_2O_3-doped)	∼0.05	–	0.31	5.97	2055	Inter-granular lateral cracks
	∼0.25	∼0.1	0.38	4.50	2987	Uniform chipping
AlN	∼0.25	–	0.12	8.00	796	Inconsistent cracks
(High pure)	∼0.05	–	0.20	5.98	1326	Inter-granular lateral cracks
	∼0.25	∼0.1	0.34	4.55	2672	Uniform chipping

*The contact radius (r) is the half-width of the track left after the scratch and is measured directly from the SEM imaging of the scratch track corresponding to the critical load F_C

*The shear strength is calculated using Equation 1 [9].

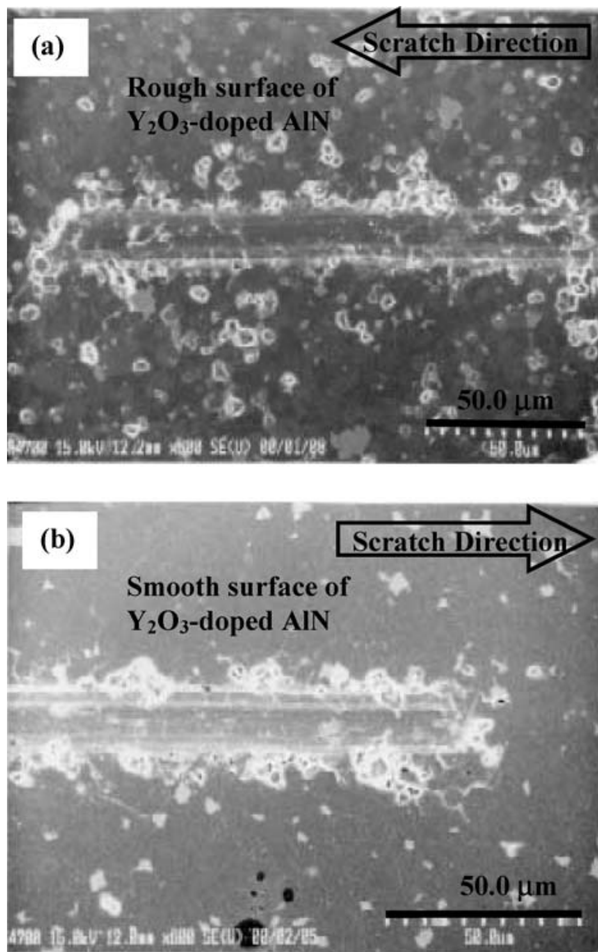

Figure 4 SEM images showing the end of the scratch tracks (F_N = 3 N) on Y_2O_3-doped AlN sample. (a) Rough surface of the sample as received, i.e., surface with pre-existing machining damages (Ra ∼0.25 μm). (b) Smooth surface removed by chemical mechanical polishing (Ra ∼0.05 μm).

where (r) is the contact radius; i.e. the half-width of the track left after the scratch.

3. Experimental results and discussions

3.1. Microscratch testing results of AlN

The microscratch experimental results are summarized in Table II, where the value of F_C is the average value for 3 tests per sample measured with a statistical deviation of ±0.01 N and the value of the shear strength is calculated using Equation 1 [9]. In Table II, the data for the contact radius (r), i.e. the half-width of the track left after the scratch were measured directly from the SEM imaging of the scratch tracks. An example of the analysis of the microscratch results of the Y_2O_3-doped AlN sample is shown in Fig. 3. This Fig. 3 shows the lateral force (F_T) and the AE signal intensity versus the normal load (F_N) curves, and the SEM micrographs of

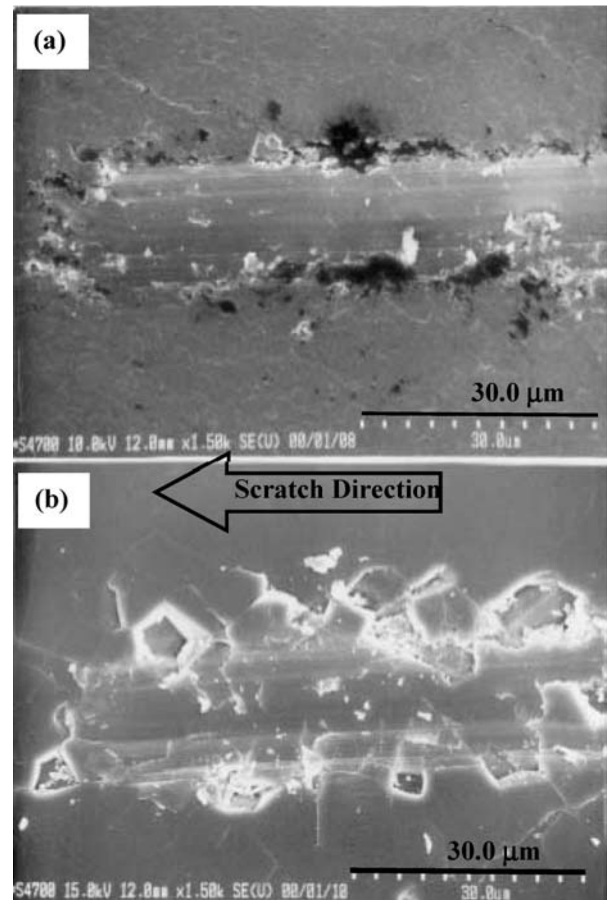

Figure 5 SEM images showing the end of the scratch tracks (F_N = 3 N) on AlN. (a) Pure AlN (3.0 μm average grain size). (b) High pure AlN (9.8 μm average grain size).

the scratch tracks corresponding to $F_N = 0.27$ N and $F_N = 3.00$ N (end of the scratch), respectively. In the AE curve shown in Fig. 3a, there are indications of a series of crack nucleation and growth events corresponding to various AE signal intensities that occur at different normal loads. As shown in Fig. 3b, the first cracks and microscopic deformation simultaneously recorded with the first variation in tangential force was observed at critical load $F_C = 0.27$ N (Fig. 3a), without clearly defined transition from ductile to fracture dominated mode scratch. It therefore appears that the diamond stylus intersected pre-existing polishing damages [5] on the surface of the AlN sample and caused low cohesive failure at $F_C = 0.27$ N. As the scratch progressed, the stylus generated more scratch damages and caused higher cohesive failure at $F_C = 0.45$ N. In Fig. 3, unlike the variation of the tangential force simultaneously recorded with the microscopic deformation of the scratch track observed using SEM imaging, the AE signal intensities were not helpful in detecting the critical load for fracture initiation and propagation during scratching the current sample. The intense AE signals, which appeared well before $F_C = 0.27$ N could be possibly attributed to fast approach and contact of the diamond stylus with the AlN sample, which exhibited pre-existing polishing surface discontinuities. Moreover, SEM imaging showed microfracture events around the scratch track in the region between 1.2 to 2.1 N and were in agreement with the variation of the lateral force. However, the AE signal intensities in this region were found lower than the ones at $F_C = 0.27$ N probably because of the crack grow during scratching is inconsistent due to the different form, length and area density of the pre-existing polishing damages.

The effect of pre-existing polishing defects on the scratch resistance of AlN was also studied. The SEM image of the scratch tracks corresponding to maximum applied normal load $F_N = 3$ N (end of scratch) on two samples of Y_2O_3-doped AlN substrates are shown in Fig. 4a and b, respectively. In Fig. 4a, the surface of

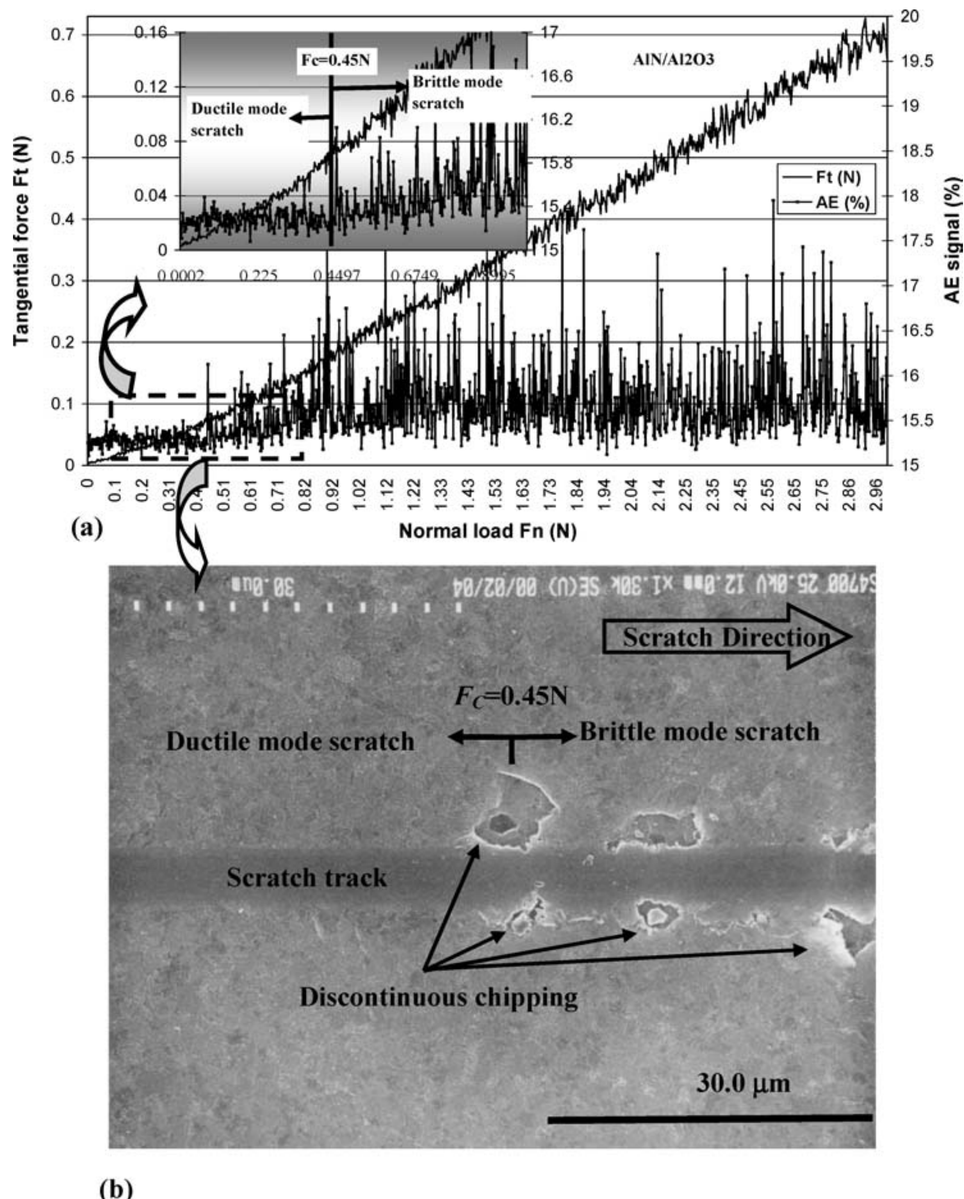

Figure 6 Results of microscratch test on AlN (pure) with Al_2O_3 (∼0.1 μm)oxide layer. (a) Lateral force (F_T) and acoustic emission signal intensity versus normal load (F_N) curves. (b) SEM image of the scratch groove showing the ductile to brittle mode scratch transition in form of uniform discontinuous chipping at recorded critical load $F_C = 0.45$ N.

the sample was rough (Ra ~0.25 μm) and exhibited pre-existing polishing defects prior to scratch testing as clearly seen around the scratch track. In this case, the critical load for crack initiation during scratching was recorded as $F_C = 0.27$ N. In Fig. 4b, the surface of the Y_2O_3-doped AlN sample was removed using chemical mechanical polishing prior to scratch experiment, i.e., most of pre-existing damages were removed from the surface (Ra ~0.05 μm) as clearly seen around the scratch track. In this case, the critical load for crack initiation was recorded as $F_C = 0.31$ N. Hence, F_C was found to decrease with increasing the surface roughness of the Y_2O_3-doped AlN because the critical load required for the propagation of pre-existing damages on a rough surface is lower than that required for crack initiation on smooth surface of the sample.

The effect of the AlN grain size on the scratch resistance of the AlN substrates was also studied. The SEM images of the scratch tracks corresponding to maximum applied normal load $F_N = 3$ N (end of scratch) on pure AlN (grain size ~3.0 μm) and high pure AlN (grain size ~9.8 μm) samples are shown in Fig. 5a and b, respectively. In Fig. 5a, the critical load for the initiation of first cracks was recorded as $F_C = 0.30$ N, while in Fig. 5b was $F_C = 0.12$ N. Besides, the damage density caused by the spherical stylus during scratching test on pure AlN (Fig. 5a) was found lesser than on high pure AlN sample (Fig. 5b). Thus, F_C and accordingly the shear strength and damage density were found to decrease with increasing the average grain size of AlN. The authors are exploring this significant result, which shows that pure AlN with small grain size has higher fracture strength and better material properties for application in semiconductor processing components.

3.2. Microscratch testing results of AlN with Al_2O_3 oxide layers

The experimental results are summarized in Table II. An example of the analysis of the microscratch results of the pure AlN with an Al_2O_3 oxide layer sample is shown in Fig. 6. This figure shows the simultaneously recorded tangential force variations and acoustic emission fluctuations (Fig. 6a) along with the SEM image showing the ductile to brittle mode scratch transition at recorded critical load $F_C = 0.45$ N (Fig. 6b).

The critical load F_C was found higher for the pure AlN with an Al_2O_3 oxide layer comparing with the pure AlN. Moreover, unlike in the case of pure AlN where F_C was found to generate inconsistent different kinds of damages, the critical load in the case of pure AlN with an Al_2O_3 oxide layer was found to generate uniform discontinuous bulky chipping. The distance between these chipping decreased and the fracture mode gradually transformed to continuous chipping failure mode as the scratch progressed as shown in Fig. 7a–d.

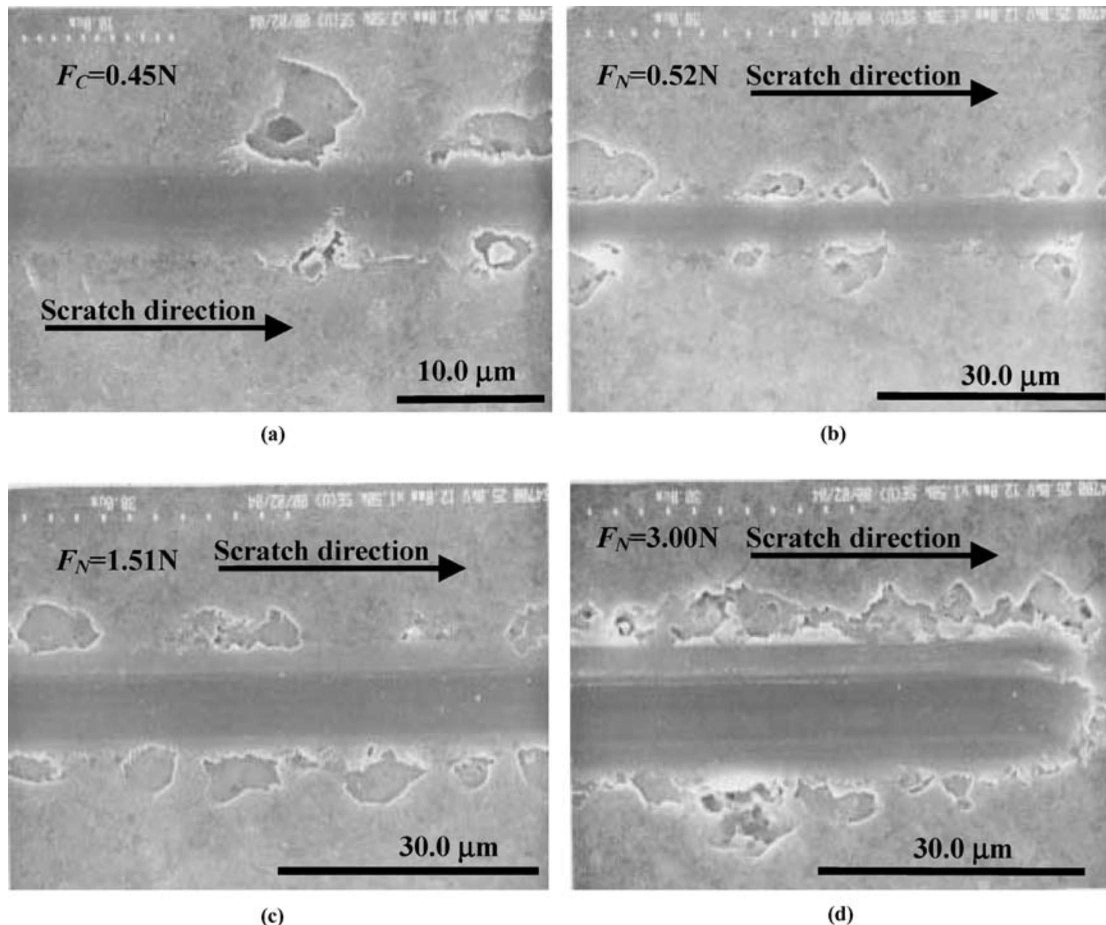

Figure 7 SEM images of a microscratch test performed in progressive loading mode on AlN (pure) with Al_2O_3 (~0.1 μm)oxide layer at different applied loads: (a) $F_C = 0.45$ N, ductile to brittle scratch transition in form of discontinuous chipping. (b) $F_N = 0.52$ N, discontinuous chipping. (c) $F_N = 1.51$ N, decrease of the distance between chippings. (d) $F_N = 3.00$ N, continuous chipping.

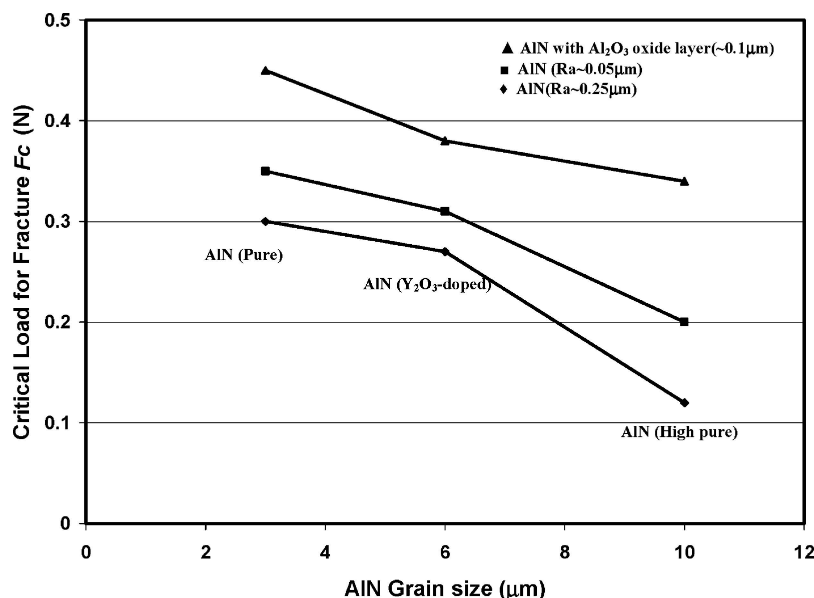

Figure 8 Relationship between the critical load for cohesive failure F_C (±0.01 N) and the average grain size of AlN for different surface topographies of the substrate.

Although the cohesive failure within the Al_2O_3 oxide layer, i.e., the transition from ductile to facture dominated scratch mode, was clearly observed at the critical load $F_C = 0.45$ N, the exposure of the substrate could not be identified by the energy dispersive spectroscopic analysis of the scratch track corresponding to this load.

4. Conclusions

The surface scratch resistance, damage evolution and damage detection during microscratching of pure AlN and AlN with an Al_2O_3 oxide layer of 0.1 μm thickness were investigated. The results of this tribological work are summarized in Fig. 8. These results make clear the effect of the surface topography and surface modification on the micromechanical properties of AlN. It was found that the surface failure mode of pure AlN was different from that of the AlN/Al_2O_3 system during scratching. Moreover, the surface modification of AlN with the use of an Al_2O_3 oxide layer was shown to improve the tribological properties of AlN and to be useful in solving the problem of defect density during processing and polishing of AlN-based EC.

As shown in Fig. 8, the measured critical load for fracture initiation and propagation F_C (and therefore the calculated shear strength) were found to decrease with increasing the grain size and surface roughness of AlN. This critical load F_C was measured as 0.30 N and was found to generate inconsistent different kinds of damages on pure AlN.

A very significant result regarding the effect of AlN's grain size and purity on the fracture strength during scratch testing is shown if Fig. 5. The authors are exploring this significant result, which shows that pure AlN with small grain size has higher fracture strength and better material properties for application in semiconductor processing components.

In the case of AlN with an Al_2O_3 (0.1 μm) oxide layer, the critical load F_C was measured as 0.45 N, higher than pure AlN, and was found to generate uniform discontinuous bulky chipping. The distance between these chippings decreased and the fracture mode gradually transformed to continuous chipping failure mode as the scratch progressed.

Acknowledgments

Financial support of this work by the Venture Business Laboratory of Akita University is gratefully acknowledged. The author would like to thank Mr. Gwenael Bollore of CSM for his discussions, Prof. Hiroshi Eda and Dr. Jun Shimizu of Ibaraki University for their support and encouragement

References

1. P. R. CHOUDHURY, "Handbook of Microlithography, Micromachining, and Microfabrication" Vol. 1 (The Society of Photo-Optical Instrumentation Engineers, Washington, 1997) p.11.
2. *Idem., ibid.* Vol. 2 (The Society of Photo-Optical Instrumentation Engineers, 1997) p. 3.
3. D. W. RICHERDSON, "Modern Ceramic Engineering: Properties, Processing, and Use in Design," 2nd edition (Marcel Dekker, New York, 1992) p. 374.
4. T. ABRAHAM and W. DAVIDSON, "GB-163 Near Net Shape Manufacturing of Advanced Ceramics" (1995) 64.
5. J. C. LAMBROPOULOS, S. D. JACOBS, B. GILLMAN, F. YANG and J. RUCKMAN, in Proceedings of the 5th Inter. Conf. on Advances in the Fusion and Processing of Glass, Vol. 82 (Ceramic Transactions, 1998) p. 469.
6. T. TSUKIZOE and T. HISAKADO, *ASME J. Lubrif. Technol.* **90F** (1968) 81.
7. D. J. WHITHOUSE, "Handbook of Surface Metrology" (The Institute of Physics, 1994) p. 792.
8. R. T. L. HOWELS and S. D. PROBERT, "Contacts Between Solids" TRG Rep., 1701 (R/X), (1968).
9. P. BENJAMIN and C. WEAVER, *Proc. R. Soc. London.* **A254** (1960) 63.
10. K. L. MITTAL, "Adhesion Measurement of Thin Films, Thick Films and Bulk Coatings" (ASTM Philadelphia, 1978) p. 5.
11. *Idem.*, "Adhesion Measurement of Films and Coatings" (VSP BV, Netherlands, 1995).
12. A. J. PERRY, *Thin Solid Films.* **78** (1981) 77.
13. *Idem.*, *ibid.* **197** (1983) 167.

14. P. A. STEINMANN, Y. TARDY and H. E. HINTERMANN, *ibid*. **154** (1987) 333.
15. P. J. BURNET and D. S. RICKERBY, *ibid.* **154** (1987) 403.
16. C. JULIA-SCHMUTZ and H. E. HINTERMANN, *Surf. Coat. Technol*. **48** (1991) 1.
17. S. J. BULL and D. S. RICKERBY, *ibid*. **42** (1990) 149.
18. T. W. WU, *J. Mater. Res*. **6** (1991) 407.
19. L. CHOUANINE, *Optical Eng*. **40** (8) (2001) 1709.
20. B. BUSHAN and B. K. GUPTA, *Adv. Info. Stor. Syst*. **6** (1995) 193.
21. AlN Ceramics for semiconductor equipments, *Ostech Electronic Mater. Catalog*, 2002.
22. K. L. RUTHERFORD and I. M. HUTCHINGS, *Surf. Coat. Technol*. **79** (1996) 231.

Received 23 December 2004
and accepted 14 March 2005